

Received December 15, 2020, accepted December 23, 2020, date of publication December 28, 2020, date of current version January 8, 2021.

Digital Object Identifier 10.1109/ACCESS.2020.3047655

# Experimental Modelling and Amplitude-Frequency Response Analysis of a Piecewise Linear Vibration System

YIXIA SUN 

School of Mechanical and Automotive Engineering, Shanghai University of Engineering Science, Shanghai 201620, China  
e-mail: sunyixia@sues.edu.cn


This work was supported by the National Natural Science Foundation of China under Grant 11602135.

**ABSTRACT** The amplitude-frequency response of a nonlinear vibration system with the coexistence of stiffness and viscous damping piecewise linearities are analysed by means of analytical, numerical and experimental investigations. First, a mechanical model of the piecewise linear system under simple harmonic base excitation is established, and the amplitude-frequency response equation is obtained by the averaging method. Second, an experimental device is built to realize the piecewise linear system. The stiffness and damping coefficients are identified by the least square method. Third, case studies are conducted to illustrate the effect of the clearance and base excitation amplitude on the amplitude-frequency response. The experimental results show that the introduction of the piecewise linear stiffness and damping significantly decreases the response amplitude at the primary resonance. The piecewise linear stiffness, damping coefficients, primary resonance frequency and frequency range of the bi-stable state depend on the clearance and excitation amplitude. The experimental results are consistent with the theoretical predictions and numerical simulation results of the method of backward differentiation formulas. This research provides instructive ideas to the design of the nonlinear isolator in practical engineering.

**INDEX TERMS** Piecewise linearity, the averaging method, stability, amplitude-frequency response, parameter identification.

## NOMENCLATURE

$m_1$	the proof mass (kg)
$t$	time (s)
$x_1$	absolute displacement of the proof mass (m)
$u$	displacement of the base excitation (m)
$x_2$	relative displacement of the proof mass (m)
$F_1$	piecewise linear restoring force (N)
$F_2$	piecewise linear damping force (N)
$\Delta$	clearance (m)
$k_1, k_2$	linear stiffness coefficient (N/m)
$c_1, c_2$	linear damping coefficient (N · s/m)
$u_0$	displacement amplitude of the base excitation (m)
$u_1$	acceleration amplitude of the base excitation (m/s <sup>2</sup> )
$\omega$	angular frequency of the base excitation (rad/s)

The associate editor coordinating the review of this manuscript and approving it for publication was Feiqi Deng .

$\Omega$	frequency of the base excitation (Hz)
$\tau$	dimensionless time
$x$	dimensionless relative displacement of the proof mass
$l$	dimensionless clearance
$\omega_1$	primary frequency characteristic
$\varepsilon g$	dimensionless base excitation characteristic
$\varepsilon \xi_1, \varepsilon \xi_2$	dimensionless damping characteristic
$\varepsilon \eta$	dimensionless stiffness characteristic
$\varepsilon f_1$	dimensionless piecewise restoring force
$\varepsilon f_2$	dimensionless piecewise damping force
$\varepsilon$	small dimensionless parameter
$a$	dimensionless relative displacement amplitude
$\beta$	phase of the dimensionless relative displacement
$\varphi$	angle of the dimensionless relative displacement
$( )'$	d( )/d $\tau$

## I. INTRODUCTION

Piecewise linear systems are systems where the stiffness or damping coefficients remain constant over a range of amplitude and dramatically change to another set of constant values once a threshold is reached [1]. In general, piecewise linear systems can be classified into two categories. The vector field of the first category is discontinuous due to the rigid constraint or dry friction. The vector field of the second category is nonsmooth but continuous, and the nonsmoothness may be caused by a clearance or elastic constraint. Piecewise linear systems have been used to represent switching circuit and resistors [2], [3], mechanical system with Coulomb friction [4], [5], gene regulatory networks [6], [7], and so on. Owing to the practical significance and wide application, a great deal of effort has been devoted to the study of piecewise linear systems over the years.

The study on piecewise linear systems dates back to the early 1930s. Den Hartog and Mikina [8] were the first scholars to find an approximate solution for periodic motion of a system with bilinear stiffness. Shaw and Holmes [9] analysed the harmonic, subharmonic and chaotic motions of a periodically forced SDOF system with a piecewise linear restoring force. Based on Shaw-Pierre nonlinear modes and Rauscher's approach, Uspensky *et al.* [10] presented a method to calculate the forced vibration of the piecewise linear systems near superharmonic resonances. Yu [11] and Ma *et al.* [12] presented Bozzak-Newmark and Bozzak-Newmark-LCP numerical schemes, respectively, to determine the responses of MDOF piecewise linear systems. Xu *et al.* [13] computed the periodic solution of a harmonically excited oscillator with both stiffness and viscous damping piecewise linearities by the incremental harmonic balance (HIB) method. Zou and Nagarajaiah [14] were the first to study a piecewise linear system with negative and positive stiffness by a modified Lindstedt-Poincaré method. For the forced vibration of an oscillator with piecewise linear asymmetrical damping, Silveira *et al.* [15] obtained the exact analytical solutions by joining the solutions for the compression and expansion phases and the approximate solutions by the HIB method. Wang *et al.* [16] studied the effect of the system parameters on the dynamical behaviours of a piecewise linear SDOF oscillator with fractional-order derivative by the averaging method.

The application of the piecewise linearity in vibration control is well developed. Deshpande *et al.* [1] proposed the optimum parameters of the primary suspension and jump-avoidance conditions of the secondary suspension for a piecewise linear vibration isolation system. Zhong and Chen [17] established the relationship between the system parameters and the topological bifurcation solution of a piecewise linear vehicle suspension. Joglekar and Mitra [18] presented piecewise linear SDOF/MDOF oscillators to represent cracked beams and employed a wavelet-based method to analyse the vibration behaviours. Based on Rauscher method and calculations of the autonomous system nonlinear modes,

Uspensky and Avramov [19], [20] studied nonlinear modes of the free and forced torsional vibrations for a piecewise linear system. Shui and Wang [21] and Mustaffer *et al.* [22] presented a dynamic vibration absorber with an adjustable piecewise linear stiffness and experimentally analysed the characteristic and performance of the absorber, respectively. Yao *et al.* [23] attached a nonlinear energy sink (NES) with piecewise linear stiffness to suppress the vibration of a forced primary vibration system, and the effectiveness of the NES was proven by experiments. In design of energy harvesters, Tien and D'souza [24] proposed a new vibration harvester composed of a piecewise linear oscillator and an adjustable gap, which has an optimal vibration performance over a broad frequency range and the best performance at resonance. Zhang *et al.* [25] experimentally designed a vibration harvester with piecewise linear stiffness characteristic, which may work in a broadband and low-frequency range. Using the methods of Floquet theory, Filippov method and finite different method, El Aroudi *et al.* [26] studied the stability and bifurcation behaviour of a piecewise linear spring-mass-damper system for vibration-based energy harvesting applications. Shi *et al.* [27] investigated the vibration transmission characteristic of the SDOF oscillator and coupled 2DOF oscillators with bilinear stiffness and bilinear damping by the harmonic balance method and numerical integrations. Dai *et al.* [28] studied the dynamic behaviour, vibration transmission and power flow of impact oscillators with linear and quasi-zero-stiffness (QZS) nonlinear constraints. Dai *et al.* [29] further revealed the effects of the design parameters and locations of the nonlinear constraints on the response and vibration transmission of impact oscillators with nonlinear motion constraints created by the diamond-shaped linkage mechanism. Narimani *et al.* [30] focused on the availability of the averaging method to find the closed-form solution for the frequency response of a piecewise linear isolator with a hard nonlinearity. The analytical result of the averaging method agreed well with both experimental results and numerical simulation.

From the above literature review, many studies have examined piecewise linear systems in terms of theoretical prediction and numerical simulation, including the analysis of stability, bifurcation, chaos motion, and amplitude-frequency characteristic. However, limited work has been done in experimental studies. In this paper, a mechanical structure with stiffness and viscous damping piecewise linearities is designed and assembled, which has the advantages of simple structure, easy implementation and low cost. Different from the research focus of Ref. [30], the objective of this paper is twofold. The first objective is to identify the piecewise linear coefficients of the built experiment model and verify the correctness of the identification results. The other objective is to discuss the effect of the clearance and base excitation amplitude on the amplitude-frequency response of the piecewise linear system by experimental verification combined with theoretical analysis and numerical calculation.

The paper is organized as follows. In Section II, the mechanical model of a SDOF piecewise linear system is presented. The amplitude-frequency response of the system is obtained by the averaging method. In Section III, the stability analysis of the steady-state response is completed through the eigenvalue analysis method. Section IV is devoted to explore the amplitude-frequency characteristic experimentally. Conclusions are given in Section V.

**II. MECHANICAL MODEL AND PERTURBATION ANALYSIS**

The mechanical model of the piecewise linear system under investigation is presented in Fig. 1(a).  $x_1$  and  $u$  are the absolute displacements of proof mass  $m_1$  and the base, respectively.  $x_2 = x_1 - u$  is the relative displacement of proof mass  $m_1$  with respect to the base.  $F_1(x_2)$  and  $F_2(dx_2/dt)$  are the piecewise linear restoring force and damping force, respectively. The stiffness and damping coefficients are illustrated in Fig. 1(b) and (c).  $\Delta$  is the clearance. The stiffness and damping coefficients are  $k_1$  and  $c_1$  for  $x_2 \leq \Delta$ . The stiffness and damping coefficients increase to  $k_2$  and  $c_2$  for  $x_2 > \Delta$ .

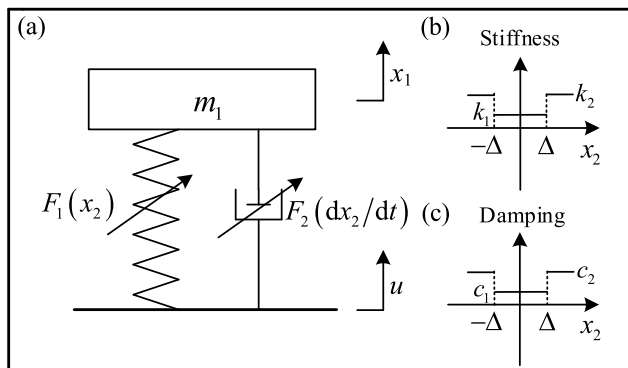


**FIGURE 1. Mechanical model of the piecewise linear system and representation of the stiffness and damping.**

According to Fig. 1, the governing differential equation of the system is

$$m_1 d^2 x_1 / dt^2 + F_1(x_2) + F_2(dx_2/dt) = 0 \tag{1}$$

$$\text{where } F_1(x_2) = \begin{cases} k_2 x_2 + (k_2 - k_1) \Delta & x_2 < -\Delta \\ k_1 x_2 & |x_2| \leq \Delta \\ k_2 x_2 - (k_2 - k_1) \Delta & x_2 > \Delta, \end{cases}$$

$$F_2(dx_2/dt) = \begin{cases} c_2 dx_2/dt & x_2 < -\Delta \\ c_1 dx_2/dt & |x_2| \leq \Delta \\ c_2 dx_2/dt & x_2 > \Delta \end{cases}$$

Assuming  $u = u_0 \sin(\omega t)$  and substituting  $x_1 = x_2 + u$  into (1), we obtain

$$m_1 d^2 x_2 / dt^2 + F_1(x_2) + F_2(dx_2/dt) = m_1 u_1 \sin(\omega t) \tag{2}$$

where  $u_1 = u_0 \omega^2$ .

To analyse the primary resonance response of the system, small damping, weak nonlinearity, and soft excitation are assumed. Letting  $x_0 = 0.01$  m, the dimensionless transform parameters are

$$\begin{aligned} \omega_1 &= \sqrt{\frac{k_1}{m_1}}, \quad \tau = \omega_1 t, \quad x = \frac{x_2}{x_0}, \quad l = \frac{\Delta}{x_0}, \\ r &= \frac{\omega}{\omega_1}, \quad \varepsilon \xi_1 = \frac{c_1}{m_1 \omega_1}, \quad \varepsilon \xi_2 = \frac{c_2}{m_1 \omega_1}, \\ \varepsilon \eta &= \frac{k_2 - k_1}{m_1 \omega_1^2}, \quad \varepsilon g = \frac{u \omega^2}{\omega_1^2 x_0}, \quad \varepsilon \delta = \frac{(k_2 - k_1) \Delta}{m_1 \omega_1^2 x_0}, \end{aligned}$$

where  $\varepsilon$  is a small dimensionless parameter.

Setting  $x' = dx/d\tau$ , the dimensionless form of (2) is

$$x'' + x + \varepsilon \xi_1 x' + \varepsilon f_1(x) + \varepsilon f_2(x') = \varepsilon g \sin(r\tau) \tag{3}$$

where

$$f_1(x) = \begin{cases} \eta x + \delta & x < -l \\ 0 & |x| \leq l \\ \eta x - \delta & x > l \end{cases} \tag{4}$$

$$f_2(x') = \begin{cases} (\xi_2 - \xi_1) x' & x < -l \\ 0 & |x| \leq l \\ (\xi_2 - \xi_1) x' & x > l \end{cases} \tag{5}$$

By the averaging method [30], the approximate solution of (3) can be written as

$$x = a \sin(r\tau + \beta) = a \sin \varphi \tag{6}$$

where  $a$  and  $\varphi$  are the functions of  $\tau$ .

The velocity is required to have the same form as the case when  $\varepsilon = 0$ , that is,

$$x' = ar \cos \varphi \tag{7}$$

Equations (6) and (7) imply that

$$a' \sin \varphi + a \beta' \cos \varphi = 0 \tag{8}$$

Differentiating (7) with respect to  $\tau$ , we have

$$x'' = a' r \cos \varphi - ar(r + \beta') \sin \varphi \tag{9}$$

Substituting for  $x'$  and  $x''$  in (3) yields

$$a' r \cos \varphi - ar(r + \beta') \sin \varphi + a \sin \varphi + \varepsilon \xi_1 ar \cos \varphi + \varepsilon f_1(a \sin \varphi) + \varepsilon f_2(ar \cos \varphi) = \varepsilon g \sin(r\tau) \tag{10}$$

Solving (8) and (10) for  $a'$  and  $\beta'$ , we obtain

$$\begin{aligned} a' r &= \frac{1}{2} (ar^2 - a + \varepsilon g \cos \beta) \sin(2\varphi) \\ &\quad - [\varepsilon f_1(a \sin \varphi) + \varepsilon f_2(ar \cos \varphi)] \cos \varphi \\ &\quad - (\varepsilon g \sin \beta + \varepsilon \xi_1 ar) \cos^2 \varphi \end{aligned} \tag{11}$$

$$\begin{aligned} a \beta' r &= (-ar^2 + a - \varepsilon g \cos \beta) \sin^2 \varphi \\ &\quad + [\varepsilon f_1(a \sin \varphi) + \varepsilon f_2(ar \cos \varphi)] \sin \varphi \\ &\quad + \frac{1}{2} (\varepsilon \xi_1 ar + \varepsilon g \sin \beta) \sin(2\varphi) \end{aligned} \tag{12}$$

Equations (11) and (12) indicate that  $a$  and  $\beta$  slowly vary with  $\tau$  for small  $\varepsilon$  and primary resonance. In other words,  $a$  and  $\beta$  hardly change during the period of oscillation  $2\pi$ , which enables us to average out the variations in  $\varphi$  in (11) and (12). Averaging these equations over the period of  $2\pi$  and considering  $a$  and  $\beta$  to be constant while performing the averaging, the following equations describing the slow variations in  $a$  and  $\beta$  are obtained:

$$a' r = \frac{1}{2\pi} ar (\varepsilon \xi_1 - \varepsilon \xi_2) [-2\varphi_0 + \pi - \sin(2\varphi_0)] - \frac{1}{2} (\varepsilon \xi_1 ar + \varepsilon g \sin \beta) \tag{13}$$

$$a\beta' r = \frac{1}{2} (-ar^2 + a - \varepsilon g \cos \beta) - \frac{2}{\pi} \varepsilon \delta \cos \varphi_0 + \frac{\varepsilon \eta a}{2\pi} [\pi - 2\varphi_0 + \sin(2\varphi_0)] \tag{14}$$

in which  $\varphi_0 = \arcsin(l/a)$ .

For the stationary solutions of (13) and (14), that is,  $a' = \beta' = 0$ , by  $\sin^2 \beta + \cos^2 \beta = 1$ , we have

$$\left\{ (-ar^2 + a) - \frac{4}{\pi} \varepsilon \delta \cos \varphi_0 + \frac{\varepsilon \eta a}{\pi} [\pi - 2\varphi_0 + \sin(2\varphi_0)] \right\}^2 + \left\{ \frac{1}{\pi} ar (\varepsilon \xi_1 - \varepsilon \xi_2) [-2\varphi_0 + \pi - \sin(2\varphi_0)] - \varepsilon \xi_1 ar \right\}^2 = (\varepsilon g)^2 \tag{15}$$

$$\beta = \arcsin \left\{ \frac{ar (\xi_1 - \xi_2) [-2\varphi_0 + \pi - (\sin 2\varphi_0)] - \pi \xi_1 ar}{\pi g} \right\} \tag{16}$$

### III. STABILITY ANALYSIS

The perturbation of the stationary solutions is assumed to be  $a = a_0 + \Delta a$  and  $\beta = \beta_0 + \Delta \beta$ , where  $a_0$  and  $\beta_0$  are the stationary solutions of (15) and (16), and  $\Delta a$  and  $\Delta \beta$  are small perturbations. Substituting  $a = a_0 + \Delta a$  and  $\beta = \beta_0 + \Delta \beta$  into (13) and (14) and applying Taylor series, the linear equations of  $\Delta a$  and  $\Delta \beta$  can be obtained:

$$\Delta a' = E_1'(a_0) \Delta a - \frac{1}{2} \varepsilon \xi_1 \Delta a - \frac{\varepsilon g \cos \beta_0}{2r} \Delta \beta \tag{17}$$

$$\Delta \beta' = \frac{\varepsilon g \cos \beta_0}{2a_0^2 r} \Delta a + \frac{\varepsilon g \sin \beta_0}{2a_0 r} \Delta \beta + E_2'(a_0) \Delta a \tag{18}$$

where

$$E_i'(a_0) = \left. \frac{dE_i(a)}{da} \right|_{a=a_0}$$

$$E_1(a) = \frac{a}{2\pi} (\varepsilon \xi_1 - \varepsilon \xi_2) [-2\varphi_0 + \pi - \sin(2\varphi_0)]$$

$$E_2(a) = -\frac{2}{ar\pi} \varepsilon \delta \cos \varphi_0 + \frac{\varepsilon \eta}{2\pi r} [\pi - 2\varphi_0 + \sin(2\varphi_0)]$$

Thus, the characteristic equation is

$$\lambda^2 + P\lambda + Q = 0 \tag{19}$$

where  $\lambda$  is the characteristic root,

$$P = -E_1'(a_0) + \frac{1}{2} \varepsilon \xi_1 - \frac{\varepsilon g \sin \beta_0}{2a_0 r}$$

$$Q = \frac{\varepsilon g \sin \beta_0}{2a_0 r} \left[ E_1'(a_0) - \frac{1}{2} \varepsilon \xi_1 \right] + \frac{\varepsilon g \cos \beta_0}{2r} \left[ E_2'(a_0) + \frac{\varepsilon g \cos \beta_0}{2a_0^2 r} \right]$$

Based on Routh-Hurwitz criterion, the stationary solutions are stable for  $P > 0$  and  $Q > 0$ ; otherwise, the solutions are unstable. We emphasize that a saddle-node-type bifurcation occurs when a real eigenvalue of (19) changes sign, which results in the jumping phenomena. When  $\omega_1 = 20\pi$  rad/s,  $\varepsilon \xi_1 = 0.01$ ,  $\varepsilon \xi_2 = 0.015$ ,  $\varepsilon g = 0.01$ ,  $\varepsilon \eta = 0.5$ , and  $\varepsilon \delta = 0.1$ , the frequency-amplitude response of the piecewise linear system compared to a linear response for primary resonance is shown in Fig. 2. From Fig. 2, the primary resonance peak is significantly reduced, and the multi-steady state arises due to the piecewise linear stiffness and damping. Additionally, the theoretical solution is consistent with the numerical solution obtained by the method of backward differentiation formulas (BDF). Thus, the averaging method can handle the presented model.

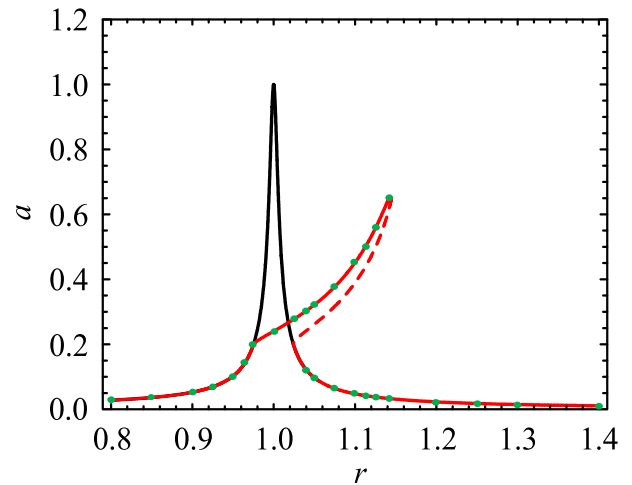


**FIGURE 2.** Frequency-amplitude response for the primary resonance (The black solid line represents the stable state for  $l = \infty$ ; the red solid and dashed lines represent the stable and unstable states derived from (15) for  $l = 0.2$ , respectively; the green dots represent the stable state by numerically solving (3)).

### IV. EXPERIMENTAL RESULTS

#### A. EXPERIMENTAL SETUP

To validate the above analysis, an experimental structure is designed and assembled as shown in Fig. 3. The proof mass 1 is attached with base 2 via five steel sheets 3 and 4. Two limiting stoppers 5 are fixed on a perforated aluminium plate 6, which are symmetrical about the middle steel sheet 4. Acceleration sensors 7 and 8 are used to measure the absolute acceleration signals of the proof mass and base, respectively.

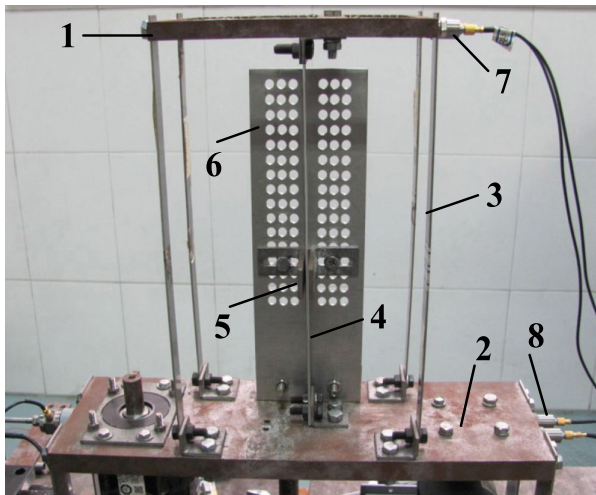


**FIGURE 3.** Photo of the experimental structure (1. proof mass, 2. base, 3. and 4. steel sheets, 5. limiting stopper, 6. perforated aluminium plate, 7. and 8. acceleration sensors).

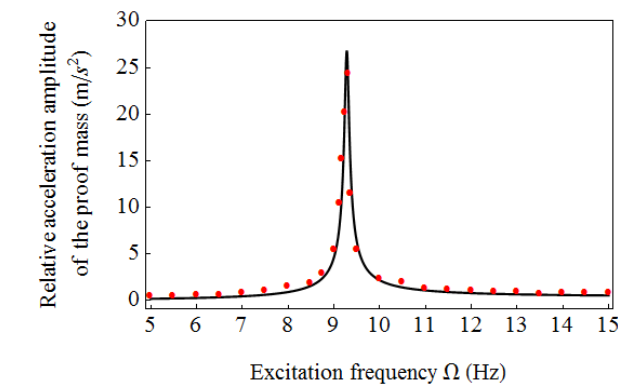
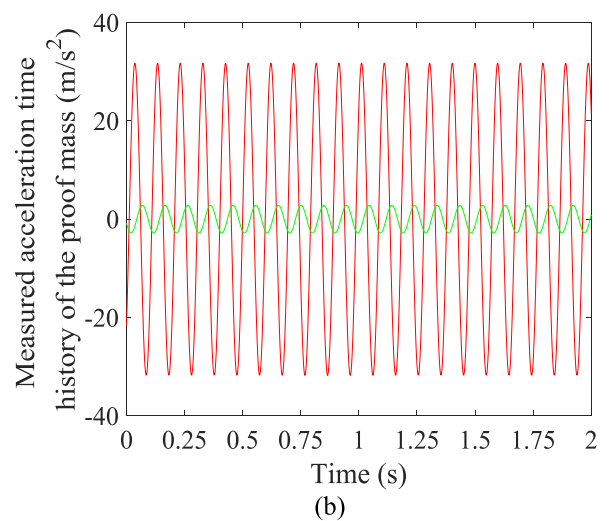
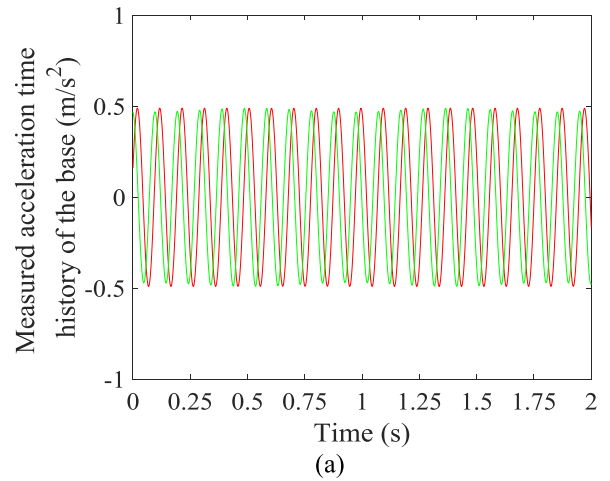


**FIGURE 4.** Frequency-amplitude response of the linear system (red dots: experimental data; black line: fitting result).

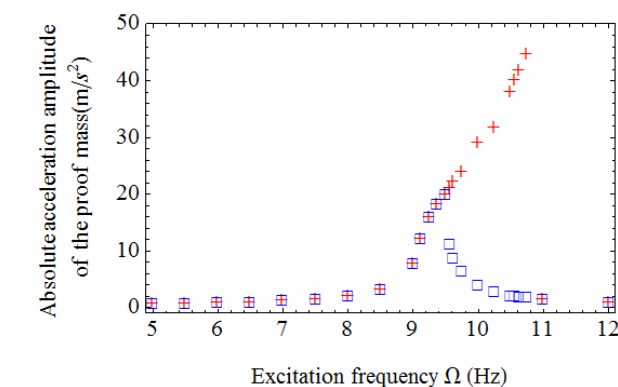


**FIGURE 5.** Experimental results of the absolute acceleration amplitude of the proof mass versus excitation frequency for  $u_1 = 0.49 \text{ m/s}^2$  and  $\Delta = 4.637 \text{ mm}$  (The marks “+” correspond to the large initial displacement  $x_1(0)$  and velocity  $dx_1(0)/dt$  of the proof mass; the marks “□” correspond to the small initial displacement  $x_1(0)$  and velocity  $dx_1(0)/dt$  of the proof mass.).

From Fig. 3, the limiting stoppers work, and the collision occurs when the relative displacement of the proof mass to the base exceeds a certain value.

**FIGURE 6.** Measured acceleration time histories for  $\Omega = 10.25 \text{ Hz}$ : (a) the base, (b) the proof mass (red and green lines correspond to large and small initial displacement  $x_1(0)$  and velocity  $dx_1(0)/dt$  of the proof mass, respectively).

The dynamical model in (1) is used to describe the vibration of the experimental structure. Some notes on the physical parameter of (1) are as follows.

(a) During the experiments, the base is harmonically excited by a shaker. The amplitude  $u_1$  and frequency  $\omega$  of the base acceleration can be adjusted by the M + p vibration controller.

(b) The value of  $\Delta$  is determined by the installation location of the two limiting stoppers.

(c)  $k_2 - k_1$  and  $c_2 - c_1$  are used to denote the deformation and energy loss during the collision, respectively. Taking (15) as the fitting model, the value of  $k_2$  and  $c_2$  can be determined to fit the experimental data by the least square method [31].

(d) As a preliminary, the values of  $m_1$ ,  $k_1$  and  $c_1$  are identified in the case of no collision. Applying sine acceleration excitation with an amplitude of  $0.294 \text{ m/s}^2$  to the base, the measured frequency-amplitude response of the linear system is recorded as the red dots shown in Fig. 4, where  $\Omega = \omega/(2\pi)$ . By the least square method, the parameters



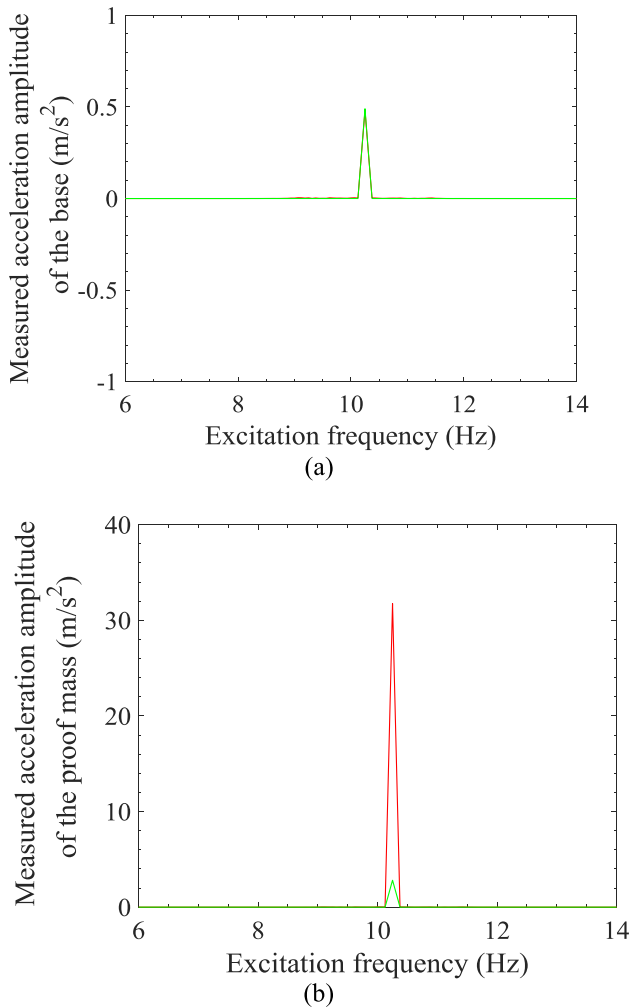


**FIGURE 7.** FFT plot of time histories from Fig. 6: (a) the base, (b) the proof mass (red and green lines correspond to large and small initial displacement  $x_1(0)$  and velocity  $dx_1(0)/dt$  of the proof mass, respectively).

are identified as  $m_1 = 0.61$  kg,  $k_1 = 2073.67$  N/m, and  $c_1 = 0.39$  N · s/m.

**B. EXPERIMENTAL RESULTS**

In the experiments, the fixed-frequency sine excitation is applied to the base. The sampling frequency is 512 Hz, and the total sampling time is 32 s. The experimental amplitude-frequency responses of the piecewise linear system are recorded and analysed at different values of the clearance  $\Delta$ , base acceleration amplitude  $u_1$  and frequency  $\Omega$ , which are compared with the theoretical and numerical values.

Case 1  $u_1 = 0.49$  m/s<sup>2</sup> and  $\Delta = 4.637$  mm

Fig. 5 shows the experimental result of the absolute acceleration amplitude of the proof mass versus excitation frequency for  $u_1 = 0.49$  m/s<sup>2</sup> and  $\Delta = 4.637$  mm. From Fig. 5, the bi-stable state exists in the frequency range [9.5625 Hz, 10.75 Hz]. In other words, the acceleration amplitude of the proof mass may dramatically decrease from the high branch to the low branch by reducing the initial displacement  $x_1(0)$  and velocity  $dx_1(0)/dt$  of the proof mass.

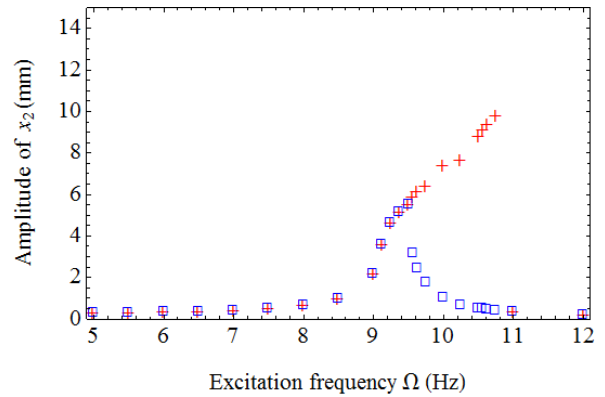


**FIGURE 8.** Experimental results of the relative displacement amplitude of the proof mass versus excitation frequency for  $u_1 = 0.49$  m/s<sup>2</sup> and  $\Delta = 4.637$  mm (The marks “+” correspond to the large initial displacement  $x_2(0)$  and velocity  $dx_2(0)/dt$  of the proof mass; the marks “□” correspond to the small initial displacement  $x_2(0)$  and velocity  $dx_2(0)/dt$  of the proof mass.).

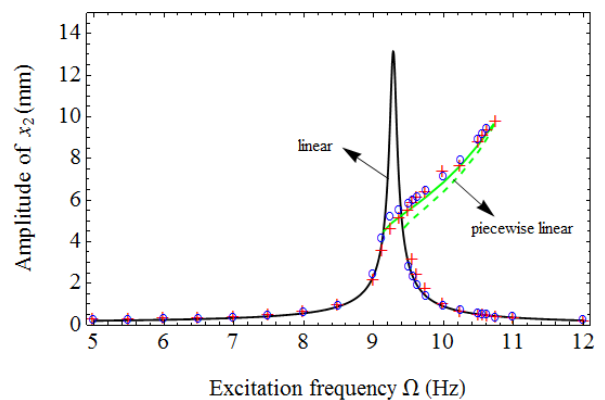


**FIGURE 9.** Comparison of the experimental, theoretical and numerical amplitude-frequency responses for  $u_1 = 0.49$  m/s<sup>2</sup> and  $\Delta = 4.637$  mm (“o”: numerical results; “+”: experimental results; green solid line: stable theoretical result; green dashed line: unstable theoretical result; black solid line: linear system).

For  $\Omega = 10.25$  Hz, the measured steady-state acceleration time histories of the system at different initial conditions are plotted in Fig. 6. Fig. 7 demonstrates the FFT plot of time histories shown in Fig. 6. In Figs. 6-7, the red and green lines correspond to the large and small initial displacement  $x_1(0)$  and velocity  $dx_1(0)/dt$  of the proof mass, respectively. From Fig. 6, with the constant acceleration amplitude of 0.49 m/s<sup>2</sup> of the base, the acceleration amplitude of the proof mass increases from 2.81 m/s<sup>2</sup> to 31.75 m/s<sup>2</sup> when the initial displacement and velocity of the proof mass increase.

By the signal processing, the experimental results of the relative displacement amplitude of the proof mass versus excitation frequency are shown in Fig. 8. Taking (15) as the fitting model to fit the experimental data shown in Fig. 8, the values of  $k_2$  and  $c_2$  are identified as  $k_2 = 3747.44$  N/m and  $c_2 = 0.560$  N · s/m by the least square method.

Fig. 9 shows the experimental amplitude-frequency response compared to the theoretical and numerical responses. The green solid and dotted lines represent the stable and unstable steady-state response given by the averaging

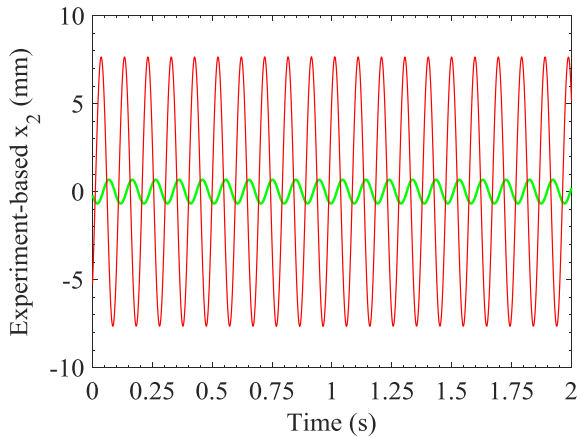


**FIGURE 10.** Experiment-based relative displacement time history for  $\Omega = 10.25$  Hz (red and green lines correspond to large and small initial displacement  $x_2(0)$  and velocity  $dx_2(0)/dt$  of the proof mass, respectively.)

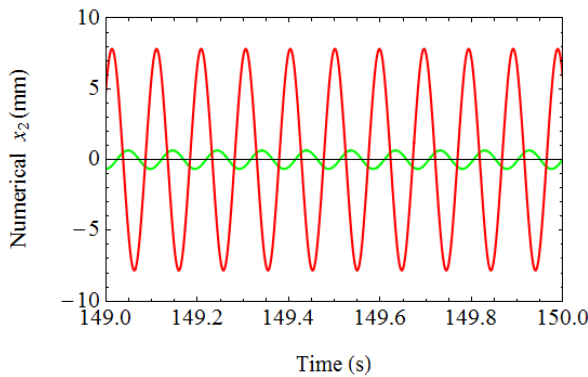


**FIGURE 11.** Numerical relative displacement time history for  $\Omega = 10.25$  Hz (red line:  $x_2(0) = 0.03$  m and  $dx_2(0)/dt = 0.02$  m/s; green line:  $x_2(0) = 0.001$  m and  $dx_2(0)/dt = 0.001$  m/s).

method. The mark “+” represents the experimental results, and “○” represents the numerical results obtained by numerically solving (2). The black solid line represents the theoretical result of the corresponding linear system (that is,  $\Delta = \infty$ ). Obviously, the experimental result is consistent with the theoretical and numerical results, which proves the correctness of the identification result. Thus, the averaging method is valid to predict the dynamical behaviour of the experimental model. From Fig. 9, the maximal relative displacement amplitude of the proof mass is reduced by 25.8% when the piecewise linearity is introduced.

For  $\Omega = 10.25$  Hz, Figs. 10 and 11 show the experiment-based and numerical relative displacement time histories of the proof mass. Comparing Figs. 10 and 11, we observe that the numerical simulation result is clearly consistent with the experimental result.

Case 2  $u_1 = 0.735$  m/s<sup>2</sup> and  $\Delta = 4.637$  mm

Similar to Case 1, the experimental result of the absolute acceleration amplitude of the proof mass versus excitation frequency is shown in Fig. 12. The observed bi-stable state is in the frequency range of [9.625 Hz, 11 Hz]. Fig. 13 shows the experimental result of the relative displacement amplitude

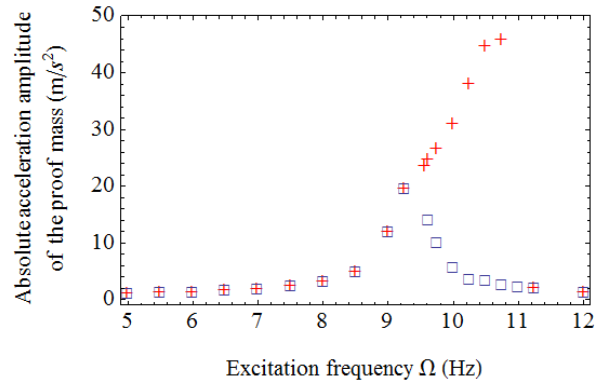


**FIGURE 12.** Experimental results of the absolute acceleration amplitude of the proof mass versus excitation frequency for  $u_1 = 0.735$  m/s<sup>2</sup> and  $\Delta = 4.637$  mm (The marks “+” correspond to the large initial displacement  $x_1(0)$  and initial velocity  $dx_1(0)/dt$  of the proof mass; the marks “□” correspond to the small initial displacement  $x_1(0)$  and initial velocity  $dx_1(0)/dt$  of the proof mass.).

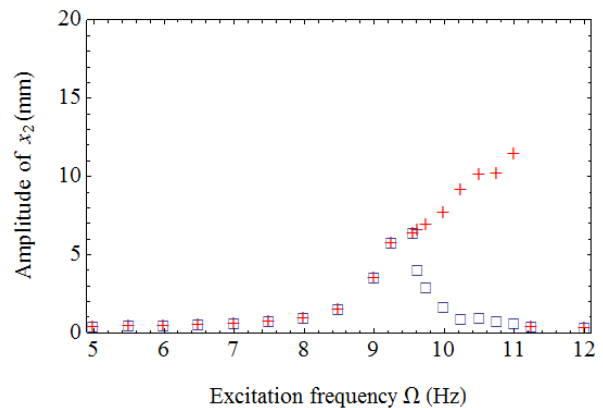


**FIGURE 13.** Experimental results of the relative displacement amplitude of the proof mass versus excitation frequency for  $u_1 = 0.735$  m/s<sup>2</sup> and  $\Delta = 4.637$  mm (The marks “+” correspond to the large initial displacement  $x_2(0)$  and velocity  $dx_2(0)/dt$  of the proof mass; the marks “□” correspond to the small initial displacement  $x_2(0)$  and velocity  $dx_2(0)/dt$  of the proof mass.).

of the proof mass versus excitation frequency. In Fig. 13, the maximum relative displacement is 11.48 mm.

Based on the experimental data in Fig. 13 and (15),  $k_2$  and  $c_2$  are calculated as  $k_2 = 3630.01$  N/m and  $c_2 = 0.766$  N · s/m. Fig. 14 displays the comparison of the experimental, theoretical and numerical results of the amplitude-frequency response. These three results are basically consistent. Compared to that of the linear system, the resonance peak of the piecewise linear system is reduced by 41.89%. Fig. 15 shows the experiment-based relative displacement time history of the proof mass for  $\Omega = 10$  Hz, which is validated by the numerical simulation shown in Fig. 16.

Case 3  $u_1 = 0.98$  m/s<sup>2</sup> and  $\Delta = 4.637$  mm

Letting  $u_1 = 0.98$  m/s<sup>2</sup> and  $\Delta = 4.637$  mm, Fig. 17 shows the change in measured absolute acceleration amplitude of the proof mass versus excitation frequency. The bi-stable state occurs in the frequency range [9.625 Hz, 11.25 Hz]. The maximum absolute acceleration amplitude is 66.46 m/s<sup>2</sup>.

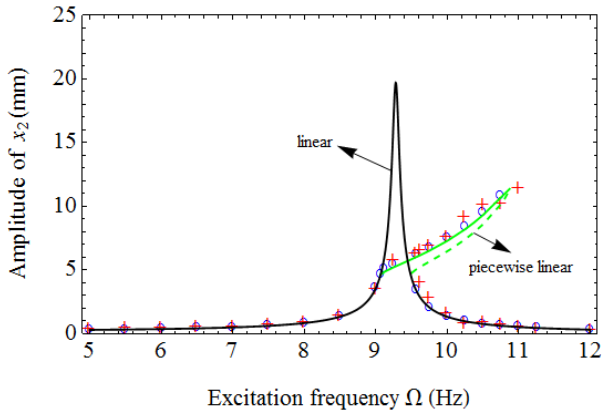


**FIGURE 14.** Comparison of the experimental, theoretical and numerical amplitude-frequency response for  $u_1 = 0.735 \text{ m/s}^2$  and  $\Delta = 4.637 \text{ mm}$  ("O": numerical results; "+" : experimental results; green solid line: stable theoretical result; green dashed line: unstable theoretical result; black solid line: linear system).

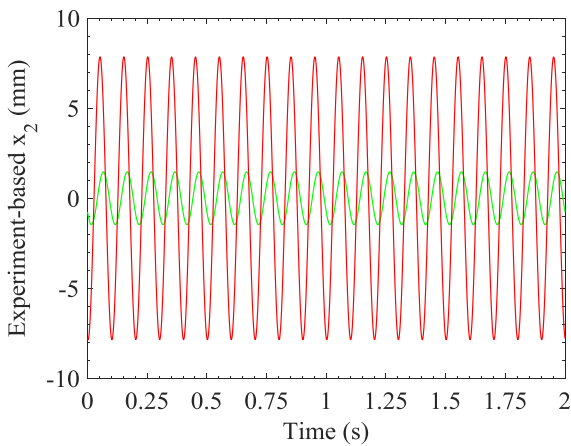


**FIGURE 15.** Experiment-based relative displacement time history for  $\Omega = 10\text{Hz}$  (red and green lines correspond to large and small initial displacement  $x_2(0)$  and velocity  $dx_2(0)/dt$  of the proof mass, respectively).

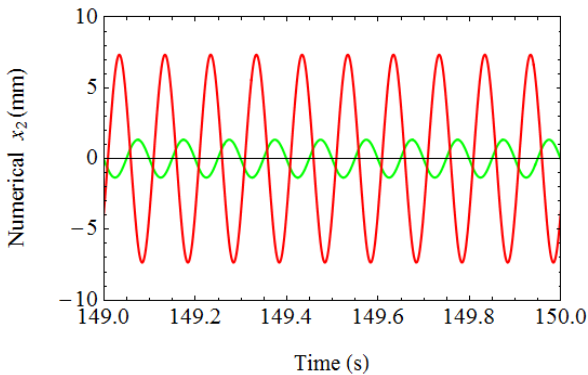


**FIGURE 16.** Numerical relative displacement time history for  $\Omega = 10 \text{ Hz}$  (red line:  $x_2(0) = 0.04 \text{ m}$  and  $dx_2(0)/dt = 0.01 \text{ m/s}$ ; green line:  $x_2(0) = 0.001 \text{ m}$  and  $dx_2(0)/dt = 0.001 \text{ m/s}$ ).

Using the experimental data in Fig. 18 and (15),  $k_2$  and  $c_2$  are determined to be  $k_2 = 3759.20 \text{ N/m}$  and  $c_2 = 0.795 \text{ N} \cdot \text{s/m}$ .

Fig. 19 shows the comparison of the experimental, theoretical and numerical results of the amplitude-frequency

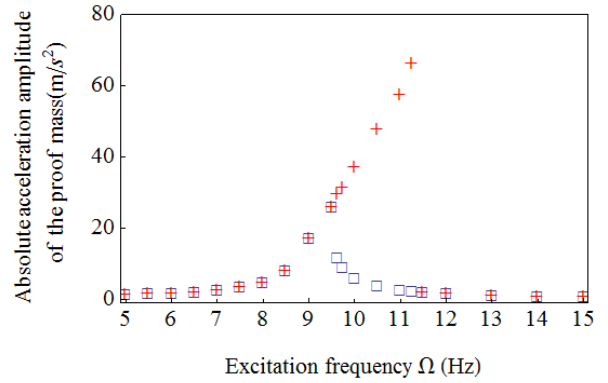


**FIGURE 17.** Experimental results of the absolute acceleration amplitude of the proof mass versus excitation frequency for  $u_1 = 0.98 \text{ m/s}^2$  and  $\Delta = 4.637 \text{ mm}$  (The marks "+" correspond to the large initial displacement  $x_1(0)$  and initial velocity  $dx_1(0)/dt$  of the proof mass; the marks "□" correspond to the small initial displacement  $x_1(0)$  and initial velocity  $dx_1(0)/dt$  of the proof mass.).

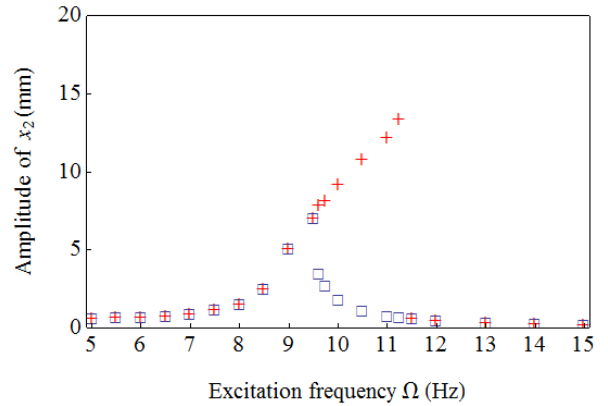


**FIGURE 18.** Experimental results of the relative displacement amplitude of the proof mass versus excitation frequency for  $u_1 = 0.98 \text{ m/s}^2$  and  $\Delta = 4.637 \text{ mm}$  (The marks "+" correspond to the large initial displacement  $x_2(0)$  and initial velocity  $dx_2(0)/dt$  of the proof mass; the marks "□" correspond to the small initial displacement  $x_2(0)$  and initial velocity  $dx_2(0)/dt$  of the proof mass.).

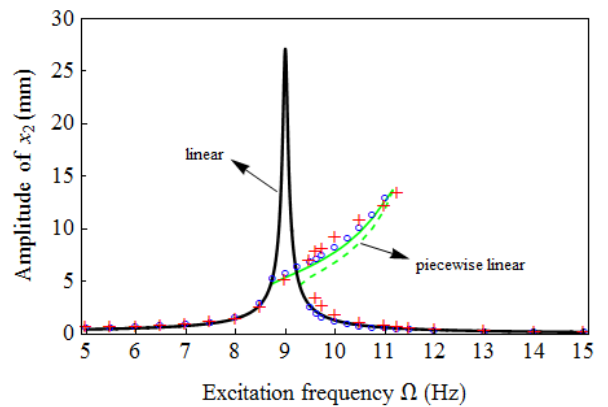


**FIGURE 19.** Comparison of the experimental, theoretical and numerical amplitude-frequency response for  $u_1 = 0.98 \text{ m/s}^2$  and  $\Delta = 4.637 \text{ mm}$  ("O": numerical results; "+" : experimental results; green solid line: stable theoretical result; green dashed line: unstable theoretical result; black solid line: linear system).

response for  $u_1 = 0.98 \text{ m/s}^2$  and  $\Delta = 4.637 \text{ mm}$ . These three results are consistent with one another. Figs. 20 and 21 show



**TABLE 1.** Effect of  $u_1$  on the experimental amplitude-frequency response of the piecewise linear system.

Case No.	$u_1$ (m/s <sup>2</sup> )	$\Delta$ (mm)	$k_2$ (N/m)	$c_2$ (N·s/m)	Primary resonant frequency (Hz)	Frequency range of bi-stable state (Hz)	Primary resonance peak (mm)	$\Psi$ (%)
1	0.49	4.637	3747.44	0.560	10.75	[9.5625,10.75]	9.79	25.80
2	0.735	4.637	3630.01	0.766	11	[9.625, 11]	11.47	41.89
3	0.98	4.637	3759.20	0.795	11.25	[9.625, 11.25]	13.40	50.77

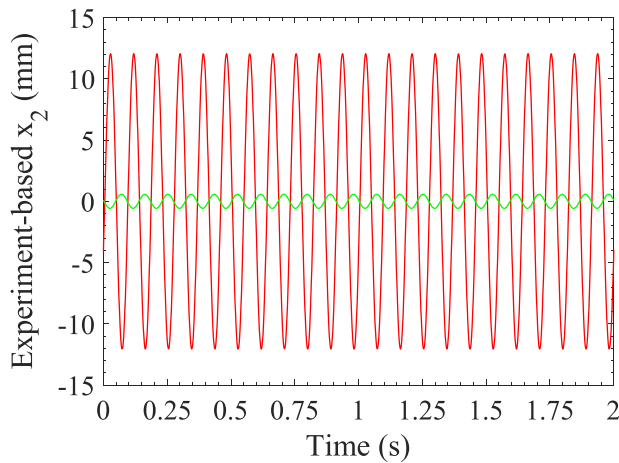


**FIGURE 20.** Experiment-based time history for  $\Omega = 11$  Hz (red and green lines correspond to large and small initial displacement  $x_2(0)$  and velocity  $dx_2(0)/dt$  of the proof mass, respectively.)

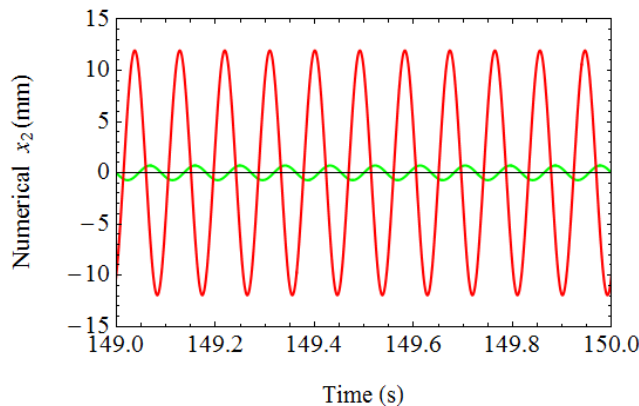
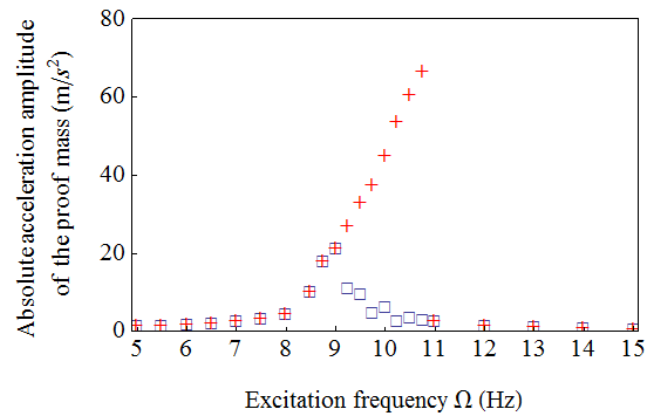


**FIGURE 21.** Numerical time history for  $\Omega = 11$  Hz (red line:  $x_2(0) = 0.04$  m and  $dx_2(0)/dt = 0.01$  m/s; green line:  $x_2(0) = 0.001$  m and  $dx_2(0)/dt = 0.001$  m/s).

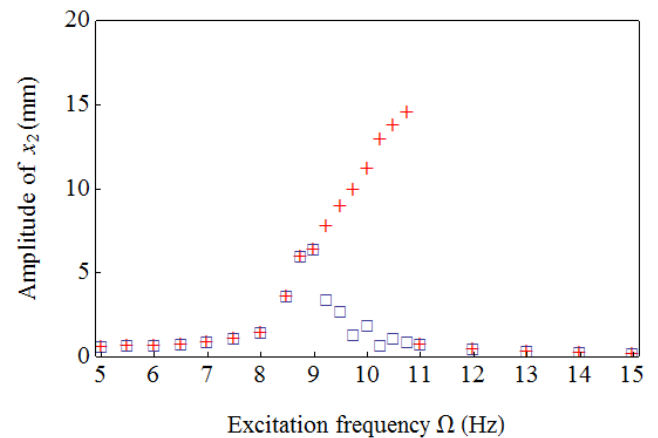
the experiment-based and numerical relative displacement time histories of the proof mass for  $\Omega = 11$  Hz, respectively. The experimental result is clearly consistent with the numerical result.

Table 1 shows the effect of  $u_1$  on the experimental amplitude-frequency response of the piecewise linear system for  $\Delta = 4.637$  mm, where  $\Psi = \frac{x_2 \max |linear - x_2 \max |piecewiselinear}{x_2 \max |linear} \times 100\%$ . As indicated in Table 1, some characteristics are summarized.

1) The primary resonance peak of the piecewise linear system is lower than that of the corresponding linear system.



**FIGURE 22.** Experimental results of the absolute acceleration amplitude of the proof mass versus excitation frequency for  $u_1 = 0.98$  m/s<sup>2</sup> and  $\Delta = 5$  mm (The marks “+” correspond to the large initial displacement  $x_1(0)$  and initial velocity  $dx_1(0)/dt$  of the proof mass; the marks “□” correspond to the small initial displacement  $x_1(0)$  and initial velocity  $dx_1(0)/dt$  of the proof mass.).



**FIGURE 23.** Experimental results of the relative displacement amplitude of the proof mass versus excitation frequency for  $u_1 = 0.98$  m/s<sup>2</sup> and  $\Delta = 5$  mm (The marks “+” correspond to the large initial displacement  $x_2(0)$  and initial velocity  $dx_2(0)/dt$  of the proof mass; the marks “□” correspond to the small initial displacement  $x_2(0)$  and initial velocity  $dx_2(0)/dt$  of the proof mass.).

In terms of engineering applications, it is beneficial for the vibration isolation.

2) Frequency range of the bi-stable state is widened, and the primary resonance frequency increases when  $u_1$  increases.

3)  $k_2$  remains basically unchanged, and  $c_2$  increases when  $u_1$  increases. Thus, the value of  $k_2$  depends on  $\Delta$ .

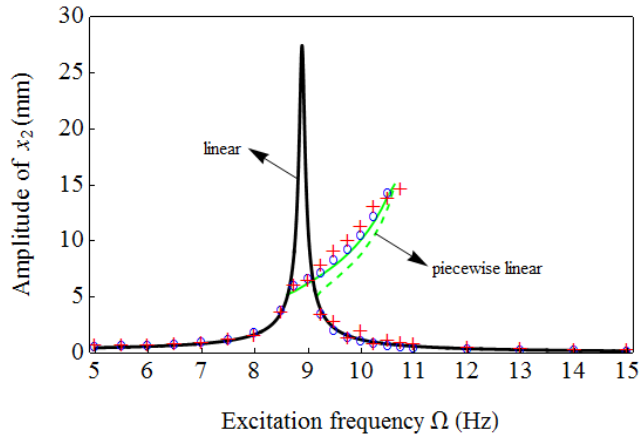


**FIGURE 24.** Comparison of the experimental, theoretical and numerical amplitude-frequency responses for  $u_1 = 0.98 \text{ m/s}^2$  and  $\Delta = 5 \text{ mm}$  ("O": numerical results; "+" : experimental results; green solid line: stable theoretical result; green dashed line: unstable theoretical result; black solid line: the linear system).

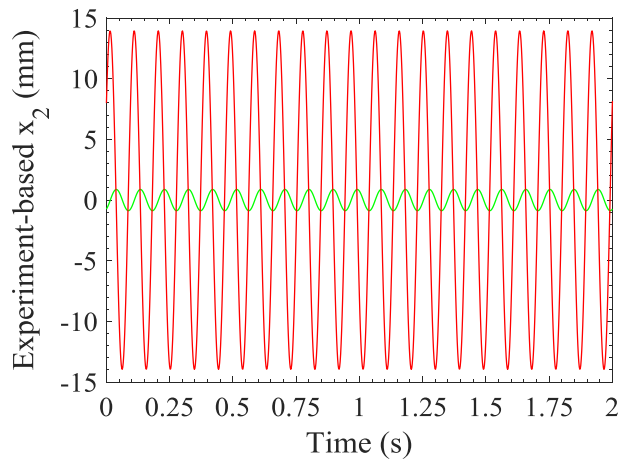


**FIGURE 25.** Experiment-based time history for  $\Omega = 10.5 \text{ Hz}$  (red and green lines correspond to large and small initial displacement  $x_2(0)$  and velocity  $dx_2(0)/dt$  of the proof mass, respectively).

The collision becomes more violent with increasing  $u_1$ , which may result in more energy loss.  $c_2$  increases accordingly.

Case 4  $u_1 = 0.98 \text{ m/s}^2$  and  $\Delta = 5 \text{ mm}$

With constant  $u_1 = 0.98 \text{ m/s}^2$  and increasing  $\Delta$ , the measured acceleration and displacement response versus the excitation frequency are shown in Figs. 22 and 23, respectively. The observed frequency range of the bi-stable state is [9.25 Hz, 10.75 Hz]. The values of  $k_2$  and  $c_2$  are determined to be  $k_2 = 3291.68 \text{ N/m}$  and  $c_2 = 0.74 \text{ N}\cdot\text{s/m}$ . The comparison of the identification results of Cases 3 and 4 indicates that increasing  $\Delta$  decreases  $k_2$  and  $c_2$ . In addition, the frequency range of bi-stable state varies with the value of  $\Delta$ .

The experimental result of the amplitude-frequency response is plotted in Fig. 24 in comparison with the numerical and theoretical responses. From Fig. 24, the primary resonance peak of the piecewise linear system is 47.33% lower than that of the linear system. The experiment-based relative displacement time history of the proof mass for  $\Omega = 10.5 \text{ Hz}$

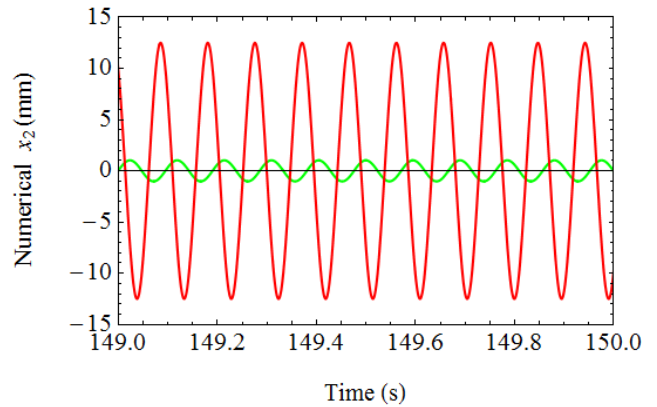


**FIGURE 26.** Numerical relative displacement time history for  $\Omega = 10.5 \text{ Hz}$  (red line:  $x_2(0) = 0.05 \text{ m}$  and  $dx_2(0)/dt = 0.01 \text{ m/s}$ ; green line:  $x_2(0) = 0.001 \text{ m}$  and  $dx_2(0)/dt = 0.001 \text{ m/s}$ ).

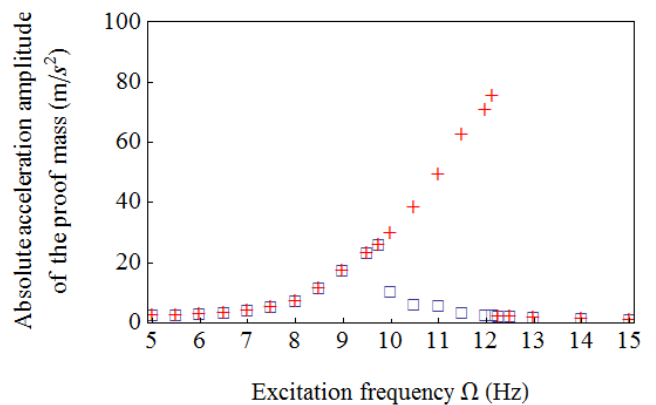


**FIGURE 27.** Experimental results of the absolute acceleration amplitude of the proof mass versus excitation frequency for  $u_1 = 1.47 \text{ m/s}^2$  and  $\Delta = 4.32 \text{ mm}$  ("+" : large initial displacement  $x_1(0)$  and initial velocity  $dx_1(0)/dt$  of the proof mass; "□" : small initial displacement  $x_1(0)$  and initial velocity  $dx_1(0)/dt$  of the proof mass).

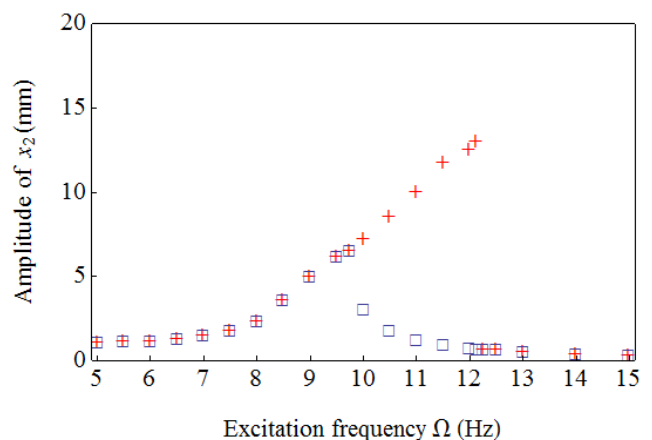


**FIGURE 28.** Experimental results of the relative displacement amplitude of the proof mass versus excitation frequency for  $u_1 = 1.47 \text{ m/s}^2$  and  $\Delta = 4.32 \text{ mm}$  (The marks "+" correspond to the large initial displacement  $x_2(0)$  and initial velocity  $dx_2(0)/dt$  of the proof mass; the marks "□" correspond to the small initial displacement  $x_2(0)$  and initial velocity  $dx_2(0)/dt$  of the proof mass).

is drawn in Fig. 25, which is constant with the numerical simulation result in Fig. 26.

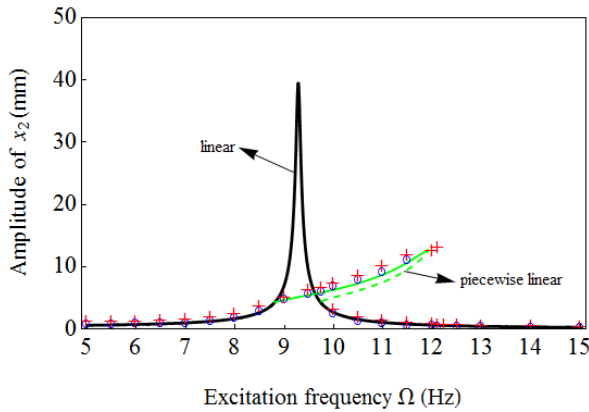


**FIGURE 29.** Comparison of the experimental, theoretical and numerical amplitude-frequency responses for  $u_1 = 1.47 \text{ m/s}^2$  and  $\Delta = 4.32 \text{ mm}$  ("o": numerical results; "+": experimental results; green solid line: stable theoretical result; green dashed line: unstable theoretical result; black solid line: the linear system).

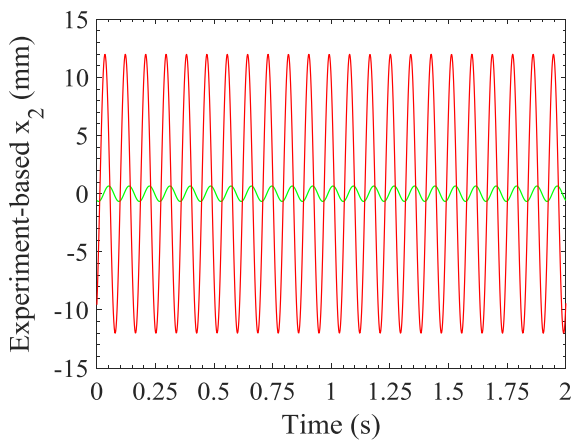


**FIGURE 30.** Experiment-based time history for  $\Omega = 11.5 \text{ Hz}$  (red and green lines correspond to large and small initial displacement  $x_2(0)$  and velocity  $dx_2(0)/dt$  of the proof mass, respectively).

Case 5  $u_1 = 1.47 \text{ m/s}^2$  and  $\Delta = 4.32 \text{ mm}$

Based the above four groups of experiments and corresponding identification results,  $k_2$  and  $c_2$  in Case 5 are predicted to be higher than those in Case 4. For  $u_1 = 1.47 \text{ m/s}^2$  and  $\Delta = 4.32 \text{ mm}$ , the measured absolute acceleration and relative displacement response versus excitation frequency are plotted in Figs. 27 and 28, respectively. The observed frequency range of the bi-stable state is [10 Hz, 12.125 Hz]. From Fig. 28, the primary resonance peak of the proof mass is 13.05 mm.  $k_2$  and  $c_2$  are identified as  $k_2 = 4400 \text{ N/m}$  and  $c_2 = 1.356 \text{ N} \cdot \text{s/m}$ , which are consistent with the prediction.

Fig. 29 shows the experimental amplitude-frequency response in comparison with the numerical and theoretical responses. From Figure 29, the maximum amplitude-frequency response in the case of piecewise linearity is reduced by 67.37% compared to that in the case of linearity.

Figs. 30 and 31 present the experiment-based and numerical relative displacement time histories of the proof mass for  $\Omega = 11.5 \text{ Hz}$ , respectively. The two results are clearly corresponded.

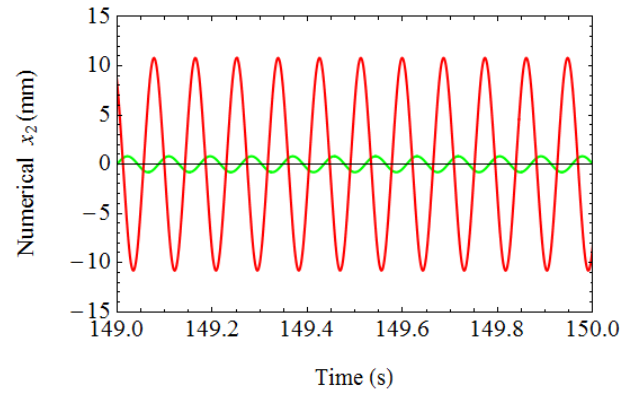


**FIGURE 31.** Numerical time history for  $\Omega = 11.5 \text{ Hz}$  (red line:  $x_2(0) = 0.04 \text{ m}$  and  $dx_2(0)/dt = 0.01 \text{ m/s}$ ; green line:  $x_2(0) = 0.001 \text{ m}$  and  $dx_2(0)/dt = 0.001 \text{ m/s}$ ).

### V. CONCLUSION

In this paper, the amplitude-frequency response of a piecewise linear system subjected to the base harmonic excitation is investigated. Based on the theoretical analysis, numerical calculation and experimental verification, the following conclusions are drawn.

(1) The analytical results given by the averaging method is consistent with the numerical and experimental results. Therefore, the averaging method is applicable to predict the dynamic behaviour of such piecewise linear system.

(2) The primary resonance response peak of the piecewise linear system is obviously less than that of the linear system. In particular, for  $u_1 = 1.47 \text{ m/s}^2$ , the primary resonance response peak at  $\Delta = 4.32 \text{ mm}$  is reduced by 67.37% compared to that at  $\Delta = \infty$ . From the viewpoint of engineering application, it may provide new ideas for the design of nonlinear isolators.

(3) The piecewise linear stiffness and damping coefficients depend on the installation location of the limiting stoppers and amplitude of the base acceleration excitation. The primary resonance frequency, primary resonance response peak and frequency range of the bi-stable state change accordingly.

(4) With the fixed installation location of the limiting stoppers (that is,  $\Delta = \text{const}$ ),  $k_2$  almost remains constant, and  $c_2$  increases with the increase in excitation amplitude. With the fixed excitation amplitude,  $k_2$  and  $c_2$  decrease with the increase in  $\Delta$ .

### ACKNOWLEDGMENT

The author would like to express their sincere thanks to the reviewers for their valuable suggestions and comments.

### REFERENCES

- [1] S. Deshpande, S. Mehta, and G. N. Jazar, "Optimization of secondary suspension of piecewise linear vibration isolation systems," *Int. J. Mech. Sci.*, vol. 48, no. 4, pp. 341–377, Apr. 2006.
- [2] L. F. Wu, Y. Guan, and Y. Liu, "Complicated behaviors and non-smooth bifurcation of a switching system with piecewise linearchaotic circuit," *Acta Phys. Sinica*, vol. 62, no. 11, Jun. 2013, Art. no. 110510.
- [3] F. Corinto, M. Gilli, and M. Forti, "Flux-charge description of circuits with non-volatile switching memristor devices," *IEEE Trans. Circuits Syst. II, Exp. Briefs*, vol. 65, no. 5, pp. 642–646, May 2018.

- [4] T. Ligurský and Y. Renard, "Bifurcations in piecewise-smooth steady-state problems: Abstract study and application to plane contact problems with friction," *Comput. Mech.*, vol. 56, no. 1, pp. 39–62, Jul. 2015.
- [5] C. Theodosiou, A. Pourmaras, and S. Natsiavas, "On periodic steady state response and stability of filippov-type mechanical models," *Nonlinear Dyn.*, vol. 66, no. 3, pp. 355–376, Nov. 2011.
- [6] V. Acary, H. de Jong, and B. Brogliato, "Numerical simulation of piecewise-linear models of gene regulatory networks using complementarity systems," *Phys. D: Nonlinear Phenomena*, vol. 269, pp. 103–119, Feb. 2014.
- [7] N. Del Buono, C. Elia, and L. Lopez, "On the equivalence between the sigmoidal approach and Utkin's approach for piecewise-linear models of gene regulatory networks," *SIAM J. Appl. Dyn. Syst.*, vol. 13, no. 3, pp. 1270–1292, Jan. 2014.
- [8] J. P. Den Hartog and S. J. Mikina, "Forced vibrations with nonlinear spring constraints," *J. Appl. Mech.*, vol. 54, pp. 157–164, Jun. 1932.
- [9] S. W. Shaw and P. J. Holmes, "A periodically forced piecewise linear oscillator," *J. Sound Vib.*, vol. 90, no. 1, pp. 129–155, Sep. 1983.
- [10] B. Uspensky, K. Avramov, and O. Nikonov, "Nonlinear modes of piecewise linear systems forced vibrations close to superharmonic resonances," *Proc. Inst. Mech. Eng., C, J. Mech. Eng. Sci.*, vol. 233, nos. 23–24, pp. 7489–7497, Dec. 2019.
- [11] S. D. Yu, "An efficient computational method for vibration analysis of unsymmetric piecewise-linear dynamical systems with multiple degrees of freedom," *Nonlinear Dyn.*, vol. 71, no. 3, pp. 493–504, Feb. 2013.
- [12] Y. L. Ma, S. D. Yu, and D. L. Wang, "Nonlinear vibrational behavior of multi-body dynamical systems with bi-directional piecewise linear spring constraints," *J. Vib. Control*, vol. 22, no. 7, pp. 1808–1819, Apr. 2016.
- [13] L. Xu, M. W. Lu, and Q. Cao, "Bifurcation and chaos of a harmonically excited oscillator with both stiffness and viscous damping piecewise linearities by incremental harmonic balance method," *J. Sound Vib.*, vol. 264, no. 4, pp. 873–882, Jul. 2003.
- [14] K. Zou and S. Nagarajaiah, "Study of a piecewise linear dynamic system with negative and positive stiffness," *Commun. Nonlinear Sci. Numer. Simul.*, vol. 22, nos. 1–3, pp. 1084–1101, May 2015.
- [15] M. Silveira, P. Wahi, and J. C. M. Fernandes, "Exact and approximate analytical solutions of oscillator with piecewise linear asymmetrical damping," *Int. J. Non-Linear Mech.*, vol. 110, pp. 115–122, Apr. 2019.
- [16] J. Wang, Y. Shen, S. Yang, Y. Lu, X. Li, and D. Zuo, "Dynamic response of a piecewise linear single-degree-of-freedom oscillator with fractional-order derivative," *J. Low Freq. Noise, Vib. Act. Control*, Sep. 2019, Art. no. 146134841987237.
- [17] S. Zhong and Y.-S. Chen, "Bifurcation of piecewise-linear nonlinear vibration system of vehicle suspension," *Appl. Math. Mech.*, vol. 30, no. 6, pp. 677–684, Jun. 2009.
- [18] D. M. Joglekar and M. Mitra, "A wavelet-based method for the forced vibration analysis of piecewise linear single- and multi-DOF systems with application to cracked beam dynamics," *J. Sound Vib.*, vol. 358, pp. 217–235, Dec. 2015.
- [19] B. V. Uspensky and K. V. Avramov, "On the nonlinear normal modes of free vibration of piecewise linear systems," *J. Sound Vib.*, vol. 333, no. 14, pp. 3252–3265, Jul. 2014.
- [20] B. Uspensky and K. Avramov, "Numerical analysis of nonlinear modes of piecewise linear systems torsional vibrations," *Meccanica*, vol. 52, no. 15, pp. 3743–3757, Dec. 2017.
- [21] X. Shui and S. Wang, "Investigation on a mechanical vibration absorber with tunable piecewise-linear stiffness," *Mech. Syst. Signal Process.*, vol. 100, pp. 330–343, Feb. 2018.
- [22] M. H. Mustaffer, R. Ramlan, M. N. Abdul Rahman, and A. Putra, "Experimental characterization and performance of dynamic vibration absorber with tunable piecewise-linear stiffness," *J. Brazilian Soc. Mech. Sci. Eng.*, vol. 42, no. 7, Jun. 2020.
- [23] H. Yao, Y. Cao, S. Zhang, and B. Wen, "A novel energy sink with piecewise linear stiffness," *Nonlinear Dyn.*, vol. 94, no. 3, pp. 2265–2275, Nov. 2018.
- [24] M.-H. Tien and K. D'Souza, "Method for controlling vibration by exploiting piecewise-linear nonlinearity in energy harvesters," *Proc. Roy. Soc. A, Math., Phys. Eng. Sci.*, vol. 476, no. 2233, Jan. 2020, Art. no. 20190491.
- [25] K. Zhang, Y. Su, J. Ding, and Z. Duan, "A low-frequency wideband vibration harvester based on piecewise linear system," *Appl. Phys. A, Solids Surf.*, vol. 125, no. 5, p. 340, May 2019.
- [26] A. El Aroudi, H. Ouakad, L. Benadero, and M. Younis, "Analysis of bifurcation behavior of a piecewise linear vibrator with electromagnetic coupling for energy harvesting applications," *Int. J. Bifurcation Chaos*, vol. 24, no. 05, May 2014, Art. no. 1450066.
- [27] B. Shi, J. Yang, and C. Rudd, "On vibration transmission in oscillating systems incorporating bilinear stiffness and damping elements," *Int. J. Mech. Sci.*, vol. 150, pp. 458–470, Jan. 2019.
- [28] W. Dai, J. Yang, and B. Shi, "Vibration transmission and power flow in impact oscillators with linear and nonlinear constraints," *Int. J. Mech. Sci.*, vol. 168, Feb. 2020, Art. no. 105234.
- [29] W. Dai and J. Yang, "Vibration transmission and energy flow of impact oscillators with nonlinear motion constraints created by diamond-shaped linkage mechanism," *Int. J. Mech. Sci.*, vol. 194, Mar. 2021, Art. no. 106212.
- [30] A. Narimani, M. E. Golnaraghi, and G. N. Jazar, "Frequency response of a piecewise linear vibration isolator," *J. Vib. Control*, vol. 10, no. 12, pp. 1775–1794, Dec. 2004.
- [31] H. Zhu, X. Rui, F. Yang, W. Zhu, and M. Wei, "An efficient parameters identification method of normalized Bouc-Wen model for MR damper," *J. Sound Vib.*, vol. 448, pp. 146–158, May 2019.



**YIXIA SUN** was born in Shandong, China, in 1983. She received the B.Eng. and M.Eng. degrees in mechanics from Shandong University, in 2006 and 2009, respectively, and the Ph.D. degree in mechanics from Tongji University, in 2015.

Since 2015, she has been a Lecturer with the Department of Machinery Manufacturing, Shanghai University of Engineering Science. Her research interests include vibration active control, dynamics of nonsmooth systems, and dynamics and control of time-delayed systems.

• • •